



1 **Enhanced Sulfate Formation in Mixed Biomass Burning and Sea-salt**
2 **Particles Mediated by Photosensitization: Effects of Chloride and**
3 **Nitrogen-containing Compounds**

4 Rongzhi Tang^{1,2}, Jialiang Ma³, Ruifeng Zhang⁴, Weizhen Cui¹, Yuanyuan Qin⁵, Yangxi Chu⁶,
5 Yiming Qin¹, Alexander L. Vogel³, Chak K. Chan^{4,*}

6 ¹ School of Energy and Environment, City University of Hong Kong, Hong Kong, China

7 ² Shenzhen Research Institute, City University of Hong Kong, Shenzhen 518057, China

8 ³ Institute for Atmospheric and Environmental Sciences, Goethe-University Frankfurt, 60438
9 Frankfurt am Main, Germany

10 ⁴ Division of Physical Science and Engineering, King Abdullah University of Science and
11 Technology (KAUST), Thuwal 23955-6900, Kingdom of Saudi Arabia

12 ⁵ College of Resources and Environment, University of Chinese Academy of Sciences, Beijing,
13 100049, China

14 ⁶ State Key Laboratory of Environmental Criteria and Risk Assessment, Chinese Research
15 Academy of Environmental Sciences, Beijing, 100012, China

16 *Correspondence to:* Chak K. Chan (chak.chan@kaust.edu.sa)

17 **Abstract**

18 Recent research has suggested that photosensitized oxidation can be an effective pathway for
19 the oxidation of SO₂ based on a limited number of model photosensitizers. However, there is a
20 notable dearth of research conducted on complex chemical systems, impeding a comprehensive
21 understanding of sulfate formation in photosensitization. This work studied sulfate formation
22 by mixing real biomass burning (BB) extracts and NaCl, mimicking internal mixtures of BB
23 and sea-salt particles. Significant enhancement of sulfate formation was observed for BB-NaCl
24 particles compared to incense burning (IS)-NaCl particles. For fresh particles, the sulfate
25 formation rate followed the trend of corn straw (CS)-NaCl>rice straw (RS)-NaCl>wheat straw
26 (WS)-NaCl>IS-NaCl. Aged particles were produced by irradiating the filters directly with UV
27 lights. Aged particles showed changes in sulfate formation rates, with the highest enhancement
28 by RS-NaCl due to interactions between RS and NaCl. Model experiments spiked with
29 nitrogen-containing organic compounds (NOCs), such as pyrazine (CHN) and 4-nitrocatechol
30 (CHON), revealed positive effects of chloride in the PS-CHON system and negative effects in
31 the PS-CHN system. Our work suggests that BB reaching or near coastal areas could affect
32 sulfate formation via photosensitizer-mediated reactions, potentially exacerbating air quality
33 concerns.

34 **Keywords:** sulfate formation, biomass burning, photosensitization, sea-salt aerosol, chloride



35 **1 Introduction**

36 Sulfate is a critical constituent of atmospheric particulate matter, exerting substantial influence
37 on atmospheric radiative forcing, air quality, and human health (Fuzzi et al., 2015; Nel, 2005;
38 Charlson et al., 1992). The commonly recognized sulfate formation mechanisms include gas-
39 phase SO₂ oxidation by OH radicals (Stockwell and Calvert, 1983) and stabilized Criegee
40 intermediates (sCIs) (Mauldin Iii et al., 2012) and multiphase and heterogeneous SO₂ oxidation
41 by H₂O₂, O₃, NO₂, organic peroxides and O₂ catalyzed transition metal ions (TMI) (Seinfeld
42 and Pandis, 2016; Wang et al., 2020a; Liu and Abbatt, 2021; Liu et al., 2020; Wang et al., 2021).
43 More recently, some new sulfate formation pathways, e.g., in-particle nitrate photolysis (Gen
44 et al., 2019b, a), triplet SO₂ chemistry (Donaldson et al., 2016; Gong et al., 2022), SO₂ oxidation
45 on acidic microdroplets (Hung and Hoffmann, 2015), photosensitizer-mediated SO₂ oxidation
46 (Tang et al., 2023; Wang et al., 2020b; Liang et al., 2022; Zhou et al., 2023; Wang et al., 2024b),
47 chlorine photoactivation (Cao et al., 2024), and enhanced chlorine and photosensitization
48 chemistry (Zhang and Chan, 2024) have been proposed. Despite extensive investigations into
49 sulfate formation mechanisms, a substantial disparity persists between modeled simulations and
50 measured sulfate concentrations, especially in marine boundary layer (Wyant et al., 2015) and
51 anthropogenic emission dominated (Wang et al., 2014), highlighting the importance to further
52 study the sulfate formation mechanism in these areas.

53 Biomass burning (BB) emits around 34-41 Tg of smoke aerosol annually, making it a significant
54 contributor to both gaseous and particulate pollutants like SO₂, primary organic aerosol (POA),
55 black carbon (BC) and brown carbon (BrC) (Schill et al., 2020; Laskin et al., 2015; Lin et al.,
56 2016; Huang et al., 2022b). The recent fire outbreaks in areas like Canada, Amazonia, and
57 Southeast Australia, together with the increased fire frequency and intensity reports in areas
58 like western US have highlighted the risks of fire, especially BB, to human and animal health
59 and climate change (Bond et al., 2013; Andreae, 2019; Jones et al., 2022). As an agricultural
60 powerhouse, China boasts immense agricultural crop yields, especially in rice, wheat, and corn
61 throughout the country. These crop residues are frequently burned in rural areas for cooking
62 and heating purposes, as well as for land preparation after harvest, resulting in the substantial
63 production of BrC (Chen et al., 2017). Atmospheric processes, e.g., atmospheric aging or long-
64 range transport, can alter the chemical compositions and optical properties of BrC, potentially
65 affecting the global climate. Recent studies have reported that the BrC species from biomass
66 burning, e.g., vanillin (VL), acetovanillone, syringaldehyde (SyrAld) can act as
67 photosensitizers and oxidize SO₂ to sulfate (Zhou et al., 2023).

68 Sea-salt aerosol, with its high particulate matter loadings and extensive surface area, is a crucial
69 atmospheric constituent that plays a significant role in interfacial and multiphase reactions with
70 reactive gases, thereby impacting global radiation balance and air quality in marine and coastal
71 areas (Gantt and Meskhidze, 2013; Chi et al., 2015). Previous studies have observed high
72 sulfate concentrations and light absorption properties in coastal regions when air masses passed
73 through inland areas due to intensive biomass burning or other anthropogenic emissions,
74 suggesting the possible interactions between the sea-salt aerosol (primarily sodium chloride)
75 and anthropogenic emissions e.g., biomass burning (Qiu et al., 2019; Huang et al., 2018; Wu et
76 al., 2022). For example, Qiu et al. (2019) discovered high absorption Ångström exponent (AAE



77 of 1.46) in coastal city Xiamen, when the air masses passing through Southeast Asia with
78 intense biomass burning. Van Pinxteren et al. (2015) observed an increase in sulfate
79 concentration ($2.26 \mu\text{g m}^{-3}$) during the RV MARIA S cruise as it approached the African
80 mainland, in contrast to the marine-origin aerosol ($1.59 \mu\text{g m}^{-3}$), showing significant influence
81 of biomass burning. Prior research has identified several secondary sulfate formation pathways
82 in sea-salt aerosol, e.g., multiphase SO_2 oxidation by O_3 (Alexander et al., 2012), coexistence
83 of NO_2 (Zhang and Chan, 2023), photosensitizers (Tang et al., 2023), chlorine-photosensitizer
84 synergistic effects (Zhang and Chan, 2024), and Cl and OH radicals generated by chlorine
85 photoactivation (Cao et al., 2024), highlighting the importance of NaCl-based photochemistry
86 in sulfate formation. Our prior study observed higher sulfate formation for incense burning-
87 NaCl particles than pure NaCl particles (Tang et al., 2023). The follow-up research found
88 magnitudes higher sulfate formation rate ($\sim 132 \mu\text{M s}^{-1}$) in premixed $\text{NH}_4\text{Cl}+\text{IC}$ (imidazole-2-
89 carboxaldehyde, a model photosensitizer found in secondary organic aerosol) particles than
90 pure NH_4Cl particles ($\sim 1.8 \mu\text{M s}^{-1}$) (Zhang and Chan, 2024). However, the studies on
91 interactions of anthropogenic emission and sea-alt aerosol on sulfate formation are very scarce.

92 In this study, we performed in-situ droplet experiments using BB extracts-NaCl mixture to
93 explore the possible interplay between biomass burning and marine aerosols in coastal areas.
94 BB was derived from the burning of rice straw (RS), wheat straw (WS), and corn straw (CS) as
95 well as incense burning (IS). This is supplemented by aqueous reactions using BB extracts and
96 bisulfite to mimic the in-cloud aqueous reactions of biomass burning emission-mediated S(IV)
97 oxidation. The effects of chloride on sulfate formation were also studied. The aims of this study
98 are to: (i) compare the differences in sulfate formation among different kinds of BB-NaCl
99 particles; (ii) evaluate the atmospheric aging (UV aging) on sulfate formation across different
100 BB-NaCl particles; (iii) Investigating the role of chloride ions in BB extracts mediated sulfate
101 formation.

102 **2 Material and methods**

103 **2.1 Burning experiments**

104 Three types of commonly used biomass (RS, WS and CS) were cut into small, uniform pieces
105 (~ 10 cm in length) and dried. About 100 g of the dried biomass materials was then introduced
106 into a traditionally iron stove commonly used in rural areas. The stove was covered with a hood
107 and the biomass was ignited using a propane lighter. The generated BB smoke was collected
108 onto 90-mm quartz filters at $0.9 \text{ m}^3 \text{ min}^{-1}$ for 10 minutes by a custom-made aerosol sampler
109 under mixed combustion condition (include flaming and smoldering, modified combustion
110 efficiency MCE, $0.85 \leq \Delta[\text{CO}_2]/(\Delta[\text{CO}_2]+\Delta[\text{CO}]) \leq 0.95$) (Ting et al., 2018). The sampler was
111 placed at a height of 1 meter above the ground and connected to a $\text{PM}_{2.5}$ sampling head through
112 a sampling pump. For incense burning (IS), laboratory generated smoldering smoke was
113 collected on 47-mm quartz filters at a flow rate of $\sim 6.0 \text{ L min}^{-1}$ for 80 min using a stainless-
114 steel combustion chamber. Note that the different combustion modes of IS and BB are
115 intentionally used to represent the real-world combustion conditions. Our previous study has
116 demonstrated the similarities (especially in sugars such as levoglucosan and phenols) in
117 GC×GC chromatograms between BB and IS (Tang et al., 2023). Hereafter, we will use BB to
118 represent both the real BB materials and the surrogate materials (IS) unless otherwise specified.



119 After sampling, the collected BB samples (fresh BB) were wrapped by pre-baked aluminum
120 foil (550 °C for 6 h) and stored at -20 °C until further analysis.

121 To achieve atmospheric aging, the collected fresh BB filter samples were put into the pre-
122 flushed (zero air, more than 24 h) combustion chamber and illuminated under UV lamps for 40
123 min. We used lamps of 185 nm and 254 nm, the combination of which have been widely used
124 in oxidation flow reactor design and experiments (Peng and Jimenez, 2020; Rowe et al., 2020;
125 Tkacik et al., 2014; Hu et al., 2022). The estimated OH exposure was $\sim 2.0 \times 10^{12}$ molecules
126 $\text{cm}^{-3} \text{ s}$, equivalent to an atmospheric aging period of 15 days (assuming an average atmospheric
127 OH concentration of 1.5×10^6 molecules cm^{-3}) (Mao et al., 2009). Detailed characterization of
128 the OH exposure can be found in our previous study (Tang et al., 2023).

129 2.2 Materials and instrumentation

130 Aqueous stock solutions of BB samples were prepared by dissolving the collected filters in
131 ultrapure water and subjecting them to ultrasonication in a cooled-water bath three times, each
132 for 20 minutes. The resulting water extracts of the BB were then filtered through 0.22 μm PTFE
133 filters and stored in brown vials at 4°C in a refrigerator. The anions, i.e., chloride, sulfate and
134 nitrate of the BB extracts were analyzed by Dionex ion chromatography (ICS 1100, CA). An
135 aliquot (~ 0.5 ml) of the BB or IS extracts were used for water-soluble organics detection by
136 ultra-high performance liquid chromatography (Thermo Scientific Dionex UltiMate 3000
137 UHPLC) coupled with high-resolution Orbitrap Fusion Lumos Tribrid mass spectrometry
138 (Orbitrap HRMS, Thermo Fisher Scientific, USA). The particulate organic matter was also
139 characterized by a thermal desorption module (TDS3, Gerstel) coupled to comprehensive two-
140 dimensional gas chromatography-mass spectrometer (GCMS-TQ™8050 NX, Shimadzu,
141 Japan). UV-Vis spectrometry (UV-3600, Shimadzu, Japan) was employed to examine the
142 absorbance of BB extracts. Total organic carbon (TOC) was measured by total carbon analyzer
143 (TOC-L CPH, Shimadzu, Japan). Metal concentrations were measured by inductively coupled
144 plasma-mass spectrometry (ICP-MS, Agilent 7800). Detailed analysis can be found in Text S1.
145 Aqueous stock solution of sodium chloride ($\geq 99.8\%$, Unichem) was prepared by dissolving the
146 corresponding salt in ultrapure water to obtain a concentration of 1M. The study utilized high
147 purity grade synthetic air and nitrogen supplied by the Linde HKO Ltd., while sulfur dioxide
148 was obtained from the Scientific Gas Engineering Co., Ltd.

149 2.3 Multiphase and aqueous-phase reactions of S(IV)

150 For SO_2 uptake experiments, the stock solution of BB extracts was premixed with sodium
151 chloride solution (1M) at a volume ratio of 1:1. A droplet generator (Model 201, Uni-Photon
152 Inc.) was then utilized to generate droplets, which were subsequently deposited onto a
153 hydrophobic substrate (model 5793, YSI Inc.) for SO_2 uptake experiments. Reactive SO_2 uptake
154 experiments were performed via a flow cell/in-situ Raman system. The top and bottom quartz
155 windows of the flow cell were used for Raman analysis and UV irradiation, respectively. The
156 light experiment was performed using a xenon lamp (model 6258, ozone free, 300W, Newport),
157 with photon flux of 9.8×10^{15} photons $\text{cm}^{-2} \text{ s}^{-1}$ in 280-420 nm received by particles in the flow
158 cell (Zhang and Chan, 2023). The relative humidity (RH) inside the flow cell was adjusted to
159 80% by mixing dry and wet synthetic air or nitrogen. The particles were then equilibrated at



160 80% RH for over 60 min and remained liquid throughout the experiment period. SO₂ was
161 introduced into the system to reach a concentration of 8.0 ppm. The prescribed size used in our
162 in-situ Raman research was 60 ± 5 μm. Despite using particles for droplet experiments that
163 were larger than ambient fine particles, we employed the SO₂ uptake coefficient (γ_{SO_2}) as a
164 kinetic parameter to account for the particle size effects. Comprehensive calculation of γ_{SO_2}
165 can be found in our previous studies (Gen et al., 2019a, b; Tang et al., 2023; Zhang et al., 2020).

166 Aqueous-phase photochemical reactions were performed using a custom-built quartz photo
167 reactor (Mabato et al., 2023; 2022). Specifically, a 500 mL solution containing 100 ppm
168 bisulfite and 1 ppm BB TOC extracts were continuously mixed using a magnetic stirrer
169 throughout the experiments. To achieve air-saturated conditions, synthetic air was continuously
170 introduced to the solutions at a flow rate 0.5 L min⁻¹ throughout the experiments. The above
171 mixed solutions were then exposed to radiation via the same xenon lamp as in the droplet
172 experiments. Samples were collected at 1hr interval for a total of 8 h for sulfate and bisulfite
173 analysis using ion chromatography.

174

175 **3 Results and Discussion**

176 **3.1 Enhanced sulfate production of BB-NaCl droplets compared to IS-NaCl droplets.**

177 Figure 1 depicts the sulfate production by (a) fresh BB-NaCl; (b) aged BB-NaCl droplets as
178 a function of time in the presence of light, air and SO₂ at 80% RH. As our previous study (Tang
179 et al., 2023) has found significantly higher sulfate formation of IS-NaCl droplets over NaCl
180 droplets, here we only focus on the comparison of sulfate formation between different kinds of
181 BB-NaCl droplets and IS-NaCl droplets. Note that sulfate concentration was normalized to the
182 initial TOC concentration of the mixture to facilitate the comparison of sulfate production of
183 different droplet compositions. Regardless of whether the extracts were fresh or aged, the
184 sulfate production by real BB-NaCl droplets was higher than IS-NaCl droplets. Specifically,
185 sulfate formed by fresh (F) BB-NaCl droplets followed the trends of CS_F-NaCl (16.8 ± 2.6 mM
186 ppmC⁻¹) > RS_F-NaCl (9.8 ± 0.1 mM ppmC⁻¹) > WS_F-NaCl (4.2 ± 0.2 mM ppmC⁻¹) > IS_F-NaCl (0.8
187 mM ppmC⁻¹) after illumination for 1080 min. In aged (A) samples, while BB_A-NaCl is more
188 efficient than IS_A-NaCl in sulfate formation, the order of sulfate formation was different from
189 the fresh samples: RS_A-NaCl (35.2 ± 0.6 mM ppmC⁻¹) > CS_A-NaCl (13.0 ± 0.1 mM ppmC⁻¹) >
190 WS_A-NaCl (6.0 ± 1.6 mM ppmC⁻¹) > IS_A-NaCl (0.6 mM ppmC⁻¹). The sulfate enhancement
191 factors of RS_F-NaCl, WS_F-NaCl, and CS_F-NaCl over IS_F-NaCl after 18 h SO₂ uptake
192 (Sulfate_{BB_F-NaCl}/IS_F-NaCl) were 11.7, 5.0 and 20.0, respectively. The enhancement of sulfate
193 can also be observed in aged BB samples, with values of 54.3, 9.2 and 20.1 for RS_A-NaCl,
194 WS_A-NaCl, and CS_A-NaCl, respectively. The lower sulfate formation of IS-NaCl droplets than
195 BB-NaCl droplets can be explained by the significantly higher TOC concentration of IS due to
196 the incomplete and smoldering combustion (Table S1). The TOC concentration of the IS
197 extracts (>550 mg L⁻¹) was nearly an order of magnitude higher than that of the BB extracts
198 (34.0-69.9 mg L⁻¹), while WSOC/(WSOC+∑anions) exhibited a more than tenfold increase in
199 BB extracts than in IS extracts. Previous studies have confirmed that the smoldering condition
200 of BB will result in significantly more organic compounds and less ions than flaming condition



201 (Wang et al., 2020c; Fushimi et al., 2017; Kalogridis et al., 2018; Kim et al., 2018). Additionally,
202 significantly higher PAHs proportion (12.2%-16.6% by intensity) than IS (~5.0%) were
203 observed by GC×GC-MS. Huang et al. (2022a) reported higher polycyclic aromatic
204 hydrocarbons (PAHs) in BB particulates (CS, WS, RS, >262.5 mg kg⁻¹, >3.7% of organic matter)
205 than in IS particulates (3.3 mg kg⁻¹, 0.9% of organic matter) (Song et al., 2023). Fushimi et al.
206 (2017) and Kim et al. (2021) demonstrated that more PAHs would be emitted under flaming
207 compared to smoldering conditions. PAHs like pyrene, fluoranthene, and phenanthrene have
208 been recognized as photosensitizers (Jiang et al., 2021; Yang et al., 2021) and are mainly from
209 combustion processes, e.g., pyrosynthesis from aliphatic and aromatic precursors in biomass
210 burning processes and the constituents vary with temperatures and oxygen contents (Pozzoli et
211 al., 2004). The higher percentage of PAHs in BB together with the collection procedure (mixed
212 combustion and higher temperature for real BB while smoldering and lower temperature for IS)
213 suggested the BB materials would generate more PAHs at high temperatures and may contribute
214 to sulfate formation.

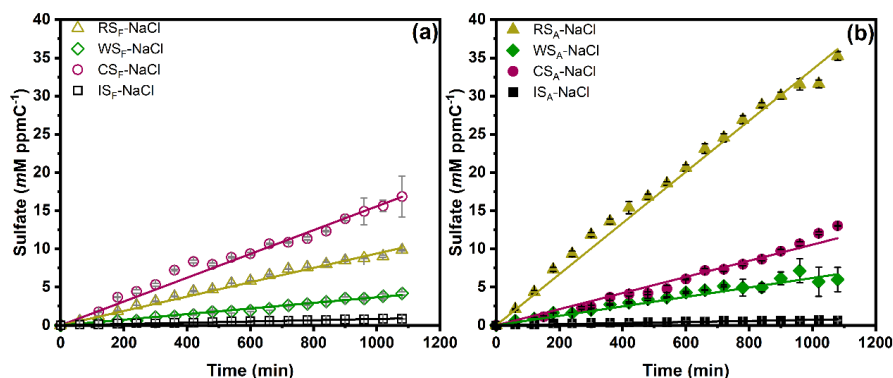
215 Table 1 presents the reactive (γ_{SO_2}) and normalized reactive SO₂ uptake coefficients ($n\gamma_{SO_2}$) of
216 different BB-NaCl droplets. Higher $n\gamma_{SO_2}$ were found for fresh and aged real BB-NaCl than
217 IS-NaCl droplets, following the trend of :CS_F-NaCl (8.8×10^{-8} ppmC⁻¹)>RS_F-NaCl (6.2×10^{-8}
218 ppmC⁻¹)>WS_F-NaCl (2.0×10^{-8} ppmC⁻¹)>IS_F-NaCl (0.61×10^{-8} ppmC⁻¹) and RS_A-NaCl ($2.2 \times$
219 10^{-7} ppmC⁻¹)>CS_A-NaCl (6.2×10^{-8} ppmC⁻¹)>WS_A-NaCl (3.5×10^{-8} ppmC⁻¹)>IS_A-NaCl (0.46
220 $\times 10^{-8}$ ppmC⁻¹), respectively.

221 In our previous study, we observed a significant increase in sulfate formation for IS-NaCl
222 droplets than NaCl droplets, which we attributed to photosensitization (Tang et al., 2023).
223 Considering the fact that BB-NaCl droplets produced sulfate more efficiently than IS-NaCl
224 droplets and NaCl droplets, we explore the underlying mechanisms driving this phenomenon.
225 Possible reasons include nitrate (from BB extracts or newly formed) photolysis, [Cl⁻-H₃O⁺-O₂]
226 photoexcitation (Cl⁻ from BB extracts), H₂O₂ oxidation, BC-catalyzed oxidation, reactive
227 nitrogen species oxidation, and organics-driven pathways e.g., HCHO, photosensitizing
228 components, organic peroxide, and TMI-organic oxidation (Ye et al., 2023).

229 Since there was no nitrate peak in our Raman spectra in all experiments, the potential impact
230 from nitrate photolysis was excluded. Besides, the significantly low Cl⁻ concentration (0.0002-
231 0.001M) in the original BB extracts (compared to 1M NaCl, Table S1) has minimized the
232 influence of chloride photoexcitation of [Cl⁻-H₃O⁺-O₂] (Cl⁻ from BB extracts) on the sulfate
233 formation. Reactive nitrogen species e.g., NO_x, HONO and NH₃ were neither introduced nor
234 detected in our system, indicating that the oxidation pathway involving reactive nitrogen
235 species as insignificant. Additionally, the water extraction process has excluded the possibility
236 of BC-catalyzed oxidation. The absence of sulfate formation in dark conditions ruled out the
237 involvement of direct H₂O₂ oxidation and organic peroxide oxidation pathways. The
238 concentrations of TMI did not exhibit a consistent relationship with the sulfate formation
239 observed in both BB_F-NaCl and BB_A-NaCl droplets (Figure S2), suggesting that the TMI-
240 catalyzed oxidation pathway may not be responsible for the observed phenomenon. Therefore,
241 the most probable reason for the enhancement of sulfate formation by BB-NaCl droplets over
242 NaCl droplets would be the photosensitizing components. State-of-the-art mass spectrometry



243 analysis including UHPLC-Orbitrap-MS and GC×GC-MS showed the existence of possible
 244 photosensitizers such as PAHs (e.g., fluoranthene, pyrene, cyclopenta[cd]pyrene, 4-
 245 methylphenanthrene, benzo[a]pyrene, perylene, Table S2) and aromatic carbonyls (SyrAld, VL,
 246 3,4-dimethoxybenzaldehyde, acetophenone, acetosyringone, Table S2). Photosensitizing
 247 components can directly or indirectly (by forming secondary oxidants in the presence of oxygen)
 248 oxidize S(IV) to S(VI). Wang et al. (2020b) proposed a direct oxidation process of S(IV) to
 249 sulfate by excited triplet states of photosensitizers (PS*). To explore the contribution of the
 250 direct PS* oxidation on sulfate formation, we performed the same sets of experiments in N₂-
 251 saturated condition, shown in Figure S3. The BB-NaCl droplets showed only direct PS*
 252 oxidation contribution of 3.6% to 22.7%, highlighting the predominant role of secondary
 253 oxidants (Tang et al., 2023). For BB_F-NaCl droplets, the contribution of direct PS* followed
 254 the trend of WS_F-NaCl (22.7%) > RS_F-NaCl (15.7%) > CS_F-NaCl (7.0%), while for BB_A-NaCl
 255 droplets, WS_A-NaCl (10.2%) > CS_A-NaCl (6.7%) > RS_A-NaCl (3.6%) was observed. In
 256 summary, regardless of whether fresh or aged, the secondary oxidants triggered by indirect PS*
 257 oxidation were the main reason for sulfate formation, highlighting the importance of O₂ in PS*
 258 mediated oxidation processes.



259

260 Figure 1. Sulfate production under different droplet compositions as a function of time: (a) fresh
 261 BB-NaCl droplets; (b) aged BB-NaCl droplets in air at 80% RH. RS, WS, CS and IS represent
 262 rice straw, wheat straw, corn straw and incense burning, respectively. The subscripts F and A
 263 represent fresh and aged, respectively.

264 Table 1. Sulfate formation rate constant ($k_{so_4^{2-}}$), reactive (γ_{SO_2}) and normalized SO₂ uptake
 265 coefficient ($n\gamma_{SO_2}$) of various particle compositions at 80% RH. Sulfate formation rate ($k_{so_4^{2-}}$)
 266 for aqueous phase reactions using different BB extracts and model compounds. 1, 10, 100 and
 267 200 represent the concentration of different compounds (in ppm).

Particle Composition	$k_{so_4^{2-}}$ ($\mu\text{M min}^{-1} \text{ppmC}^{-1}$)	γ_{SO_2}	$n\gamma_{SO_2}^a$ ppmC ⁻¹
RS _F -NaCl	9.4 ± 0.10	(2.2 ± 0.023) × 10 ⁻⁶	(6.2 ± 0.066) × 10 ⁻⁸
WS _F -NaCl	3.7 ± 0.048	(0.66 ± 0.0086) × 10 ⁻⁶	(2.0 ± 0.027) × 10 ⁻⁸



CS _F -NaCl	15.6 ± 0.11	(2.0 ± 0.015) × 10 ⁻⁶	(8.8 ± 0.065) × 10 ⁻⁸
IS _F -NaCl	0.83 ± 0.011	(1.7 ± 0.034) × 10 ⁻⁶	(0.61 ± 0.012) × 10 ⁻⁸
RS _A -NaCl	33.5 ± 0.38	(6.6 ± 0.074) × 10 ⁻⁶	(21.5 ± 0.24) × 10 ⁻⁸
WS _A -NaCl	6.2 ± 0.18	(0.92 ± 0.027) × 10 ⁻⁶	(3.5 ± 0.10) × 10 ⁻⁸
CS _A -NaCl	10.6 ± 0.23	(1.0 ± 0.023) × 10 ⁻⁶	(6.2 ± 0.13) × 10 ⁻⁸
IS _A -NaCl	0.72 ± 0.026	(1.3 ± 0.052) × 10 ⁻⁶	(0.46 ± 0.017) × 10 ⁻⁸
Aqueous Reactions	Concentration (ppm)	$k_{so_4^{2-}}$ (ppm min ⁻¹)	$k_{so_4^{2-}}$ (μM min ⁻¹)
RS _F	1	0.31	3.2
RS _F -NaCl	1-100	0.16	1.6
RS _F -NaCl	1-200	0.085	0.9
WS _F	1	0.19	2.0
CS _F	1	0.25	2.6
IS _F	1	0.19	2.0
RS _A	1	0.33	3.4
RS _A -NaCl	1-100	0.37	3.8
RS _A -NaCl	1-200	0.63	6.4
WS _A	1	0.26	2.7
CS _A	1	0.33	3.4
IS _A	1	0.080	0.82
NaCl	100	0.051	0.52
NaCl	200	0.079	0.81
SyrAld	1	0.15	1.5
SyrAld-Pyz	1-1	0.68	7.1
SyrAld-Pyz-NaCl	1-1-10	0.67	6.9
SyrAld-Pyz-NaCl	1-1-100	0.55	5.7
SyrAld-Pyz-NaCl	1-1-200	0.50	5.2
SyrAld-4-NC	1-1	0.11	1.1
SyrAld-4-NC-NaCl	1-1-10	0.13	1.4
SyrAld-4-NC-	1-1-100	0.13	1.4



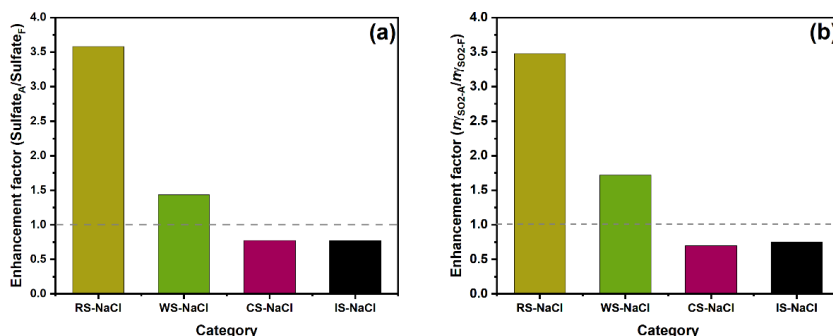
NaCl			
SyrAld-4-NC-NaCl	1-1-200	0.15	1.5
SyrAld-NaCl	1-10	0.11	1.1
SyrAld-NaCl	1-100	0.17	1.8
SyrAld-NaCl	1-200	0.17	1.7
VL	1	0.26	2.7
VL-Pyz	1-10	0.61	6.4
VL-Pyz-NaCl	1-1-10	0.55	5.8
VL-Pyz-NaCl	1-1-100	0.43	4.5
VL-Pyz-NaCl	1-1-200	0.42	4.3
VL-4-NC	1-1	0.17	1.7
VL-4-NC-NaCl	1-1-10	0.22	2.3
VL-4-NC-NaCl	1-1-100	0.27	2.7
VL-4-NC-NaCl	1-1-200	0.23	2.4
VL-NaCl	1-10	0.25	2.6
VL-NaCl	1-100	0.26	2.7
VL-NaCl	1-200	0.28	2.9

^aThe γ_{SO_2} was normalized by the initial TOC concentration (ppmC), i.e., $n\gamma_{SO_2} = \gamma_{SO_2}/TOC$

268

269 3.2 Aging effects on sulfate formation across various BB materials

270 To investigate the aging effects across various BB materials, we aged the collected BB filters
 271 by irradiating with UV lights (185 nm and 254 nm) (Tang et al., 2023). Figure S4 exhibits the
 272 differences in sulfate formation rates of different fresh and aged BB materials. RS and WS show
 273 sulfate formation enhancement, while CS and IS show reduction after aging. Figure 2(a) shows
 274 that the 18h sulfate enhancement factor ($Sulfate_A/Sulfate_F$) followed the trend of RS-NaCl
 275 (3.6) > WS-NaCl (1.4) > CS-NaCl (0.8) \approx IS-NaCl (0.8), which is neither consistent with the
 276 trends of sulfate formation for BB_F -NaCl nor BB_A -NaCl, indicating that aging processes have
 277 different influence on sulfate formation towards BB materials. A similar trend was found for
 278 $n\gamma_{SO_2}$, showing the highest and lowest sulfate enhancement for RS-NaCl (3.5) and IS-NaCl
 279 (0.7), respectively.



280

281 Figure 2. Enhancement factor of (a) sulfate and (b) normalized SO₂ uptake coefficient $n_{\gamma_{SO_2}}$
 282 between fresh and aged BB-NaCl droplets.

283 We also performed aqueous reactions using fresh/aged BB extracts to investigate the aging
 284 effects on the sulfate formation (Figure S7). The sulfate formation rate ($k_{SO_4^{2-}}$) for different BB
 285 extracts during initial photoinduced experiments ranged from 0.8 to 3.4 $\mu\text{M min}^{-1}$. The $k_{SO_4^{2-}}$
 286 obtained in bulk-phase reactions were a magnitude lower than that of the droplets (Table 1),
 287 which is consistent with previous studies (Wang et al., 2024b; Zhang and Chan, 2024). Wang
 288 et al. (2024b) discovered sulfate formation rate magnitudes higher at air-water interface (AWI)
 289 than conventional bulk-phase reactions. They attributed this to accelerated electron transfer
 290 process at AWI, where $^3\text{PS}^*$ ($^3\text{HULIS}^*$ in their case) can accept electrons from HSO_3^- in a more
 291 efficient way due to their incomplete solvent cages. Zhang and Chan (2024) fitted a ~ 3 orders
 292 of magnitude higher rate constant of $\text{IC}^* + \text{Cl}^-$ ($\sim 10^8 \text{ M}^{-1}\text{s}^{-1}$) in particle phase than bulk-phase
 293 rate constant ($\sim 10^5 \text{ M}^{-1}\text{s}^{-1}$) (Gemayel et al., 2021; Woods et al., 2020). They attributed the
 294 enhanced sulfate formation to the expedited reactions between $^3\text{PS}^*$ and chloride ions to form
 295 reactive chlorine species, facilitated by the decreased solvation of chloride and $^3\text{PS}^*$ at the AWI
 296 (Zhang and Chan, 2024). Many studies have demonstrated that chloride ions, bisulfite ions and
 297 surfactant-like PS have the propensity to reside at the AWI of droplets, primarily driven by
 298 polarization interactions. This promotes enlarged bond dipole moments and ordered alignment
 299 of reactant molecules, resulting in reduced entropy and heightened free energy of the initial
 300 state (Jungwirth and Tobias, 2002, 2006; Ruiz-Lopez et al., 2020; Tinel et al., 2016; Yan et al.,
 301 2016; Fu et al., 2015). Other factors, e.g., S(IV) concentration (8 ppm gaseous SO₂ in droplet
 302 experiment and 100 ppm HSO_3^- in aqueous reactions), and the addition of NaCl (1M NaCl
 303 addition in droplets and no NaCl addition in aqueous reactions) may also contribute to the high
 304 sulfate formation rate in droplet experiments. In this study, the more efficient sulfate formation
 305 in droplet experiments than bulk solutions can potentially be attributed to the accelerated
 306 reactions induced by photosensitizers at the AWI, intensity variance in droplets and aqueous
 307 solution, concentrations difference in S(IV) and the addition of NaCl. However, the detailed
 308 mechanisms of the accelerated sulfate formation in droplets than bulk are still uncertain and out
 309 of the scope of this paper, and more research should be performed in the future.

310 In bulk experiments, all BB extracts have higher $k_{SO_4^{2-}}$ after aging. The increased sulfate
 311 formation of BB extracts after aging may be due to changes in their chemical compositions.



312 Compared to RS_F (28.3% for CHON- and 67.3% for CHN+ in total intensity), RS_A has higher
313 CHON- (36.1%) and CHN+ (88.3%) percentages. Zhao et al. (2022) observed a slight increase
314 in CHON percentage for RS from 53.4% to 56.2% after aging. Similar trend was observed for
315 CS extracts, where CHON- and CHN+ percentage increases from 26.7% and 65.2% to 31.5%
316 and 68.8%, respectively, after aging. As chromophoric compounds are present in brown carbon
317 (BrC) (Laskin et al., 2015), we constrained the DBE values ($0.5c \leq DBE \leq 0.9c$) to semi-
318 qualitatively distinguish chromophores in the dissolved BrC (Lin et al., 2018). Higher amounts
319 of CHON- species were found in RS_{A-BrC} (41.9%) and CS_{A-BrC} (35.5%) than RS_{F-BrC} (32.3%)
320 and CS_{F-BrC} (34.7%). One of the key categories of CHON- is nitrated aromatics, which have
321 been widely identified in lab-generated BB smoke (Huang et al., 2022b; Wang et al., 2017a;
322 Zhang et al., 2022; Xie et al., 2019) and field campaigns (Salvador et al., 2020; Mohr et al.,
323 2013; Chen et al., 2022). A series of CHON- species, e.g., $C_6H_5NO_3$, $C_6H_5NO_4$, $C_7H_7NO_3$, and
324 $C_8H_9NO_3$, which were tentatively identified as nitrophenol, nitrocatechol, methyl-nitrophenol,
325 and dimethyl-nitrophenol, have been detected in our BB extracts. Nitrophenols photolysis has
326 been found to be a potential source of OH radicals (Sangwan and Zhu, 2018; Guo and Li, 2023;
327 Cheng et al., 2009; Sangwan and Zhu, 2016). Therefore, the increase in sulfate formation by
328 RS_A and CS_A may partially be related to the more oxidants generated by nitrophenol photolysis.

329 Approximately 80% of the CHN+ species identified exhibited a diatomic nitrogen composition
330 in their molecular formula. The precise determination of the molecular structures of these
331 compounds solely based on elemental composition is challenging due to the presence of stable
332 isomers. However, the N-bases, which contain two nitrogen atoms, can be attributed to various
333 N-heterocyclic alkaloids. For example, homologs of $C_5H_6N_2(CH_2)_n$ were likely pyrazine,
334 pyrimidine or amino pyridine, which were composed of six-membered heterocyclic rings with
335 N atoms and alkyl side chains (Lin et al., 2012; Laskin et al., 2009). $C_5H_8N_2(CH_2)_n$ were likely
336 alkyl-substituted imidazole compounds, featuring a five-membered heterocyclic ring with two
337 nitrogen atoms as the core structure and alkyl side chains (Lin et al., 2012; Laskin et al., 2009).
338 For $C_7H_6N_2(CH_2)_n$ homologs, the core skeleton was $C_7H_6N_2$, with an AI_{mod} of 0.8, indicating its
339 distinctive characteristics of compounds containing fused five-membered and six-membered
340 rings, such as benzimidazole or indazole (Wang et al., 2017b). Redox-inactive heterocyclic
341 nitrogen-containing bases, e.g., pyridine, imidazole, and their derivatives, have been shown to
342 enhance the redox activity of humic-like substances (HULIS) fraction by hydrogen-atom
343 transfer, with the degree of enhancement directly correlated to their concentration (Dou et al.,
344 2015; Kipp et al., 2004). Thus, the increased CHN+ percentage may also contribute to the
345 enhanced sulfate formation of RS_A and CS_A by acting as a H-bond acceptor to facilitate the
346 $^3PS^*$ -mediated oxidation by generating more oxidants.

347 However, the CHON- and CHN+ percentages in WS_A were lower than WS_F , indicating that the
348 sulfate enhancement in WS_A was not due to the CHON and CHN species. Instead, CHO-
349 accounted for higher proportion in WS_A (68.5%) and WS_{A-BrC} (68.9%) than WS_F (65.0%) and
350 WS_{F-BrC} (64.8%). This aligns with a prior AMS study, showing increased CHO proportions in
351 aged wheat burning emissions (Fang et al., 2017). We suppose that CHO- compounds,
352 particularly photosensitizing compounds with carbonyl groups, would explain the difference of
353 sulfate formation in WS extracts (Gómez Alvarez et al., 2012; Mabato et al., 2023; Felber et al.,
354 2020; Fu et al., 2015). Therefore, we filtered the chemical formula of CHO- species from



355 UHPLC-Orbitrap-HRMS by applying maximum carbonyl ratio (MCR) (Zhang et al., 2021),
356 H/C, O/C as well as modified aromaticity index (AI_{mod}) to focus on potential photosensitizers
357 (Zhrebker et al., 2022; Koch and Dittmar, 2006). In short, molecular formula were classified
358 into six groups, namely, condensed aromatics ($AI_{mod} \geq 0.67$), polyphenolics ($0.50 < AI_{mod} < 0.67$),
359 highly unsaturated and phenolic compounds ($AI_{mod} \leq 0.5$, $H/C < 1.5$), aliphatics ($H/C \geq 1.5$,
360 $O/C \leq 0.9$, $N=0$), peptide-like compounds ($H/C \geq 1.5$, $O/C \leq 0.9$, $N > 0$) and sugar-like compounds
361 ($H/C \geq 1.5$, $O/C > 0.9$), details can be found in Text S1. As aliphatics, peptide-like compounds
362 and sugar-like compounds are unlikely to be photosensitizers, we exclude them as potential PS.
363 By applying a data filtration process involving CHO-, condensed aromatics, polyphenolics,
364 highly unsaturated and phenolic compounds based on the criteria abovementioned, and
365 $MCR \geq 0.9$, 52.6% and 49.7% of the compounds (by intensity) were selected by WS_A and WS_F ,
366 respectively. The main compositional difference lies in polyphenolics, comprising 26.3% and
367 21.8% of WS_A and WS_F respectively. Therefore, the higher sulfate formation in WS_A may be
368 related to the higher contributions of the polyphenolics, e.g., $C_8H_8O_3$.

369 3.3 Effects of Chloride and Nitrogen-containing Species on Sulfate Formation

370 Unlike the droplet experiments where RS-NaCl has the highest sulfate enhancement factor after
371 aging, aqueous reaction results (without NaCl) show a sulfate enhancement trend of
372 $WS > CS > RS > IS$, suggesting that chloride may take effect in the droplet experiments, especially
373 in RS-NaCl system. Therefore, bulk reaction experiments using rice straw (RS) extracts as an
374 example were performed with 100-200 ppm NaCl additions, where the NaCl to TOC ratio
375 ranged from 100:1 to 200:1 to match the 100:1 to 1000:1 range in droplet experiments, in order
376 to evaluate the effects of chloride on sulfate formation. Interestingly, incorporating NaCl
377 yielded contrasting results for RS_F and RS_A (Figure 3). While the addition of NaCl enhanced
378 sulfate formation in RS_A , it showed the opposite trend in RS_F . The nature of the cations and
379 ionic strength may affect the sulfate formation rate; however, previous studies have indicated
380 that their effects are negligible (Zhang and Chan, 2024; Parker and Mitch, 2016). The opposite
381 effect of the NaCl addition on RS_F and RS_A , to some extent, explain the significantly higher
382 sulfate and SO_2 uptake coefficient enhancement factor for RS-NaCl in Fig. 2. Compared to the
383 RS-based system, NaCl control experiment showed minimum (but non-zero) sulfate formation
384 (Table 1 and Figure 3). On one hand, it confirmed that chloride participated in the sulfate
385 formation in bulk reactions, possibly by forming Cl and OH radicals in the presence of air and
386 water (Cao et al., 2024; Tang et al., 2023; Zhang and Chan, 2024). On the other hand, the
387 opposite trend of Cl^- effects on RS_F and RS_A reflects its complex interactions with BB extracts
388 under light and air. While direct reaction between S(IV) species and triplet states of
389 photosensitizers (PS^*) may occur (Wang et al., 2020b), other pathways, i.e., interactions among
390 halide ions, photosensitizers and oxygen should also be considered. PS in BB extracts can
391 absorb solar radiation and form triplet-state photosensitizer ($^3PS^*$), which can then react with
392 molecular oxygen and form singlet-state oxygen $^1O_2^*$ through energy transfer. $^3PS^*$ can also
393 react with H-donor, typically organic acids (RH, e.g., vanillic acid, succinic acid, azelaic acid,
394 glutaric acid, sorbic acid, salicylic acid, Table S3) through H transfer reactions, and form a ketyl
395 radical (PSH^*) and an alkyl or phenoxy radical (R^*). PSH^* and R^* can then participate in a series
396 of reactions to form OH^* , HO_2^* , H_2O_2 and $O_2^{\cdot-}$. In the presence of a large excess of Cl^- , Cl^- can
397 act as an electron donor, and react with $^3PS^*$, forming a Cl^* and a deprotonated ketyl radical



398 (PS^{*}) (Jammoul et al., 2009). Further reactions are similar to the abovementioned reactions,
399 including the formation of reactive chlorine species (RCS, i.e., Cl[•], Cl₂[•] and ClOH[•]) and
400 reactive oxygen species (ROS, i.e., OH[•], HO₂[•], H₂O₂ and O₂[•]). These RCS and ROS
401 simultaneously contribute to S(IV) oxidation to S(VI) (Zhang and Chan, 2024).

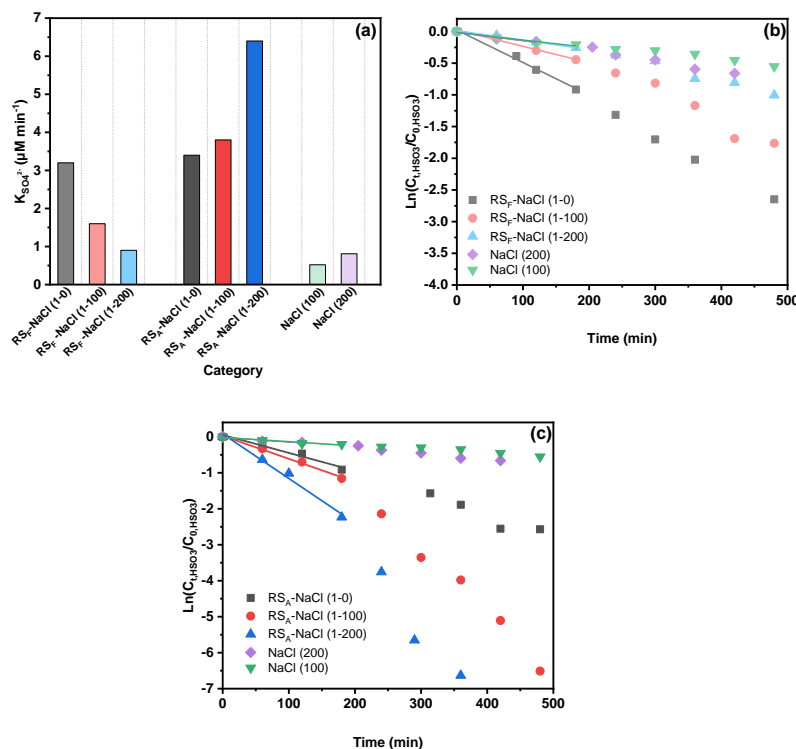
402 Statistical analysis using the Pearson correlation coefficient revealed that the concentrations of
403 CHO, CHON, and CHN species exhibited significant correlations ($|R| > 0.5$) with the sulfate
404 formation rate ($p < 0.05$, Figure S9). As PS can be the main CHO species contributing to sulfate
405 formation, N-containing organic compounds (NOCs), i.e., CHN and CHON species, may affect
406 the chloride contribution on sulfate formation rate. Therefore, we selected SyrAld and VL as
407 model CHO (PS), pyrazine (Pyz) as a model CHN, and 4-nitrocatechol (4-NC) as a model
408 CHON to elucidate how potential chemical compounds can alter the effects of chloride on
409 sulfate formation rate by studying the CHO+Cl⁻, CHO+CHN+Cl⁻, and CHO+CHON+Cl⁻
410 systems. For SyrAld and VL, as the $[Cl^-]_0/[PS]_0$ increases, $k_{so_4^{2-}}$ initially decreases and then
411 increases. The initial decrease of $k_{so_4^{2-}}$ may be attributed to the quenching of ³PS* by electron
412 transfer from Cl⁻ or loss of OH radicals by forming ClOH[•] through reaction of OH[•]+Cl⁻↔ClOH[•]
413 (Anastasio and Newberg, 2007). Excessive chloride (e.g. 100 and 200 ppm) may generate Cl
414 and OH radicals through photoexcitation in the presence of air and water and compensate for
415 the loss of ³PS* or OH radicals. Previous studies have shown controversial influence of halides
416 on the photosensitized oxidation of organic compounds or bisulfite. Parker and Mitch (2016)
417 and Zhang et al. (2023) attributed the significantly higher photodegradation of dienes,
418 thioethers and acetaminophen to the formation of reactive halogen species generated by the
419 reactions of PS and halides. Zhang and Chan (2024) reported that $[Cl^-/PS]_0$ in the range of 1:2
420 to 4:1 did not lead to significant difference in sulfate formation, possibly due to the insufficient
421 Cl⁻ concentration in triggering the interplay between PS and Cl⁻. The differences between the
422 current results and the aforementioned study might be attributed to the higher $[Cl^-/PS]_0$ (up to
423 1:200) which may have been sufficient to initiate the relevant reactions, as well as the difference
424 in photosensitizing capacities of the PS studied (triplet quantum yield of 0.86 ± 0.05 for 2-IC
425 and 0.21 ± 0.01 for VL) (Felber et al., 2021; 2020). Safiarian et al. (2023) reported that
426 increasing chloride concentrations facilitated anthracene photosensitization by producing high-
427 level reactive oxygen species (ROS). Wang et al. (2023a) found that the effects of chloride on
428 sulfate formation depended on the specific PS: enhancing sulfate production for benzophenone
429 (BP) and 3,4-dimethoxybenzaldehyde (DMB), but decreasing it for 1,4-naphthoquinone.

430 When incorporating CHN species, a 2-3-fold $k_{so_4^{2-}}$ was observed, due to the enhanced H
431 transfer by CHN acting as H-bond acceptor (Dou et al., 2015). With the addition of NaCl, the
432 enhanced H-transfer effect by CHN was inhibited, possibly due to the consumption of ³PS* by
433 Cl⁻. The addition of model CHON species into PS decreased $k_{so_4^{2-}}$, due to the consumption of
434 ³PS* by CHON species, in agreement with Wang et al. (2023b) who reported increased effective
435 quantum yield of 4-NC when co-photolysis with VL. Further addition of NaCl increased the
436 $k_{so_4^{2-}}$, possibly due to the consumption of 4-NC by RCS (Wang et al., 2024a), which, to some
437 extent, reduced the loss of ³PS*. Generally, the addition of chloride increased $k_{so_4^{2-}}$ of PS-
438 CHON but decreased $k_{so_4^{2-}}$ of PS-CHN. However, the ambient air is characterized by the
439 presence of tens of thousands of chemical compounds. As a result, the interplay among this
440 diverse array of species may occur in ways that exceed current understanding, necessitating



441 additional research to investigate the interactions between different organic compounds more
442 thoroughly.

443



444

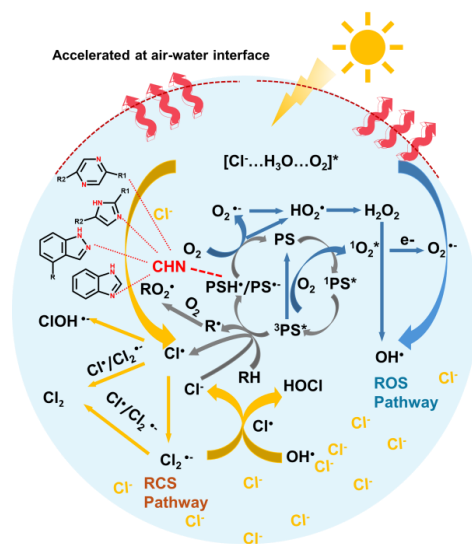
445 Figure 3. (a) Sulfate formation rate and (b) (c) bisulfite decay in RS-NaCl system. 1-0, 1-100, and
446 1-200 refer to the concentration ratios of TOC_{RS} and NaCl, in which 1, 100, 200 represent 1 ppm,
447 100 ppm and 200 ppm, respectively.

448 3.4 Proposed mechanism for sulfate formation

449 A conceptual diagram of PS and chloride mediated ROS and RCS production in the oxidation
450 of S (IV) to S (VI) was shown in Fig. 4. Initially, the photosensitizers (PS, e.g., SyrAld and VL)
451 absorb solar radiation and produce the singlet state $^1PS^*$, which then undergo a spin conversion
452 through intersystem crossing, leading to the formation of the triplet state $^3PS^*$. The $^3PS^*$ can
453 react with molecular oxygen through energy transfer and generate singlet state $^1O_2^*$, while the
454 $^3PS^*$ returns to ground state. The $^1O_2^*$ can then transform to $O_2^{\cdot-}$ via electron transfer. The
455 $^3PS^*$ can also react with an H donor (RH, e.g., organic acids, syringol, guaiacol, Table S3),
456 leading to the formation of alkyl or phenoxy radical (R^{\cdot}) and a ketyl radical (PSH^{\cdot}). R^{\cdot} can react
457 with O_2 and form RO_2^{\cdot} radicals while PSH^{\cdot} can transfer an H atom to O_2 and form HO_2^{\cdot} ,
458 returning to its ground state PS. Additionally, $^3PS^*$ can react with an electron donor, e.g., Cl^- ,



459 and form chlorine radicals and PS^* . The formed PS^* then reacts with O_2 and form O_2^* , which
460 undergoes a series of reactions and form HO_2^* , H_2O_2 and OH^* . The above-mentioned reactions
461 are the main processes in ROS pathway. Recently, Zhang and Chan(2024) have proposed that
462 the reactive chlorine species (RCS) would contribute to sulfate formation. Cao et al. (2024)
463 proposed a mechanism of OH and Cl radicals formation by $[Cl-H_3O^+-O_2]$ under light irradiation
464 through an electron transfer process. Our results also demonstrate that the addition of Cl^- will
465 affect the oxidation process of S(VI) (Figures 3, S10-S12). Combining the above, the RCS
466 pathway was shown in yellow arrows in Figure 4. The Cl^* can be formed in two pathways,
467 photoexcitation of the $[Cl-H_3O^+-O_2]$ complex that generates Cl radicals in deliquescent BB-
468 NaCl droplets or aqueous BB-NaCl solution (Cao et al., 2024), and PS^* mediated Cl^* formation
469 via electron transfer by Cl^- (Corral Arroyo et al., 2019). The formed Cl^* can then react with each
470 other through radical-radical reactions and produce molecular Cl_2 . The Cl^* can also react with
471 Cl^- or Cl_2^* , forming Cl_2^* or Cl_2 . Cl^* and Cl_2^* can also react with OH and form HOCl. $^3PS^*$
472 itself can also oxidize the S(IV) (e.g., dissolved SO_2 or bisulfite) to S(VI). However,
473 significantly lower sulfate formation was found in the presence of N_2 compared to air condition
474 (Figure S3), highlighting the importance of secondary oxidants compared to direct PS^*
475 oxidation. As a consequence, these reactive species, e.g., $OH^*/HO_2^*/O_2^*$ and Cl^*/Cl_2^* may all
476 participate in the oxidation of S(IV) to S(VI). In addition, the nitrogen-containing heterocyclic
477 compounds such as pyrazine can act as H-bonding acceptor and facilitate the H transfer, which
478 then generates more ROS (Dou et al., 2015). In light of the absence of substantial fluctuations
479 in chloride concentration (Figure S13 and S14, insignificant chloride concentration change was
480 found even in 10 ppm NaCl addition), it is postulated that chloride ions may function as a
481 reactive medium rather than as direct reactants. In this proposed scenario, the Cl radicals and
482 Cl_2^* intermediates generated during the reaction subsequently undergo reversion back to Cl^-
483 ions, thereby maintaining a relatively constant Cl^- concentration throughout the experimental
484 observations. Note that although ROS and RCS pathways both contribute to the oxidation from
485 S(IV) to S(VI), they may act as competitive relationships due to the co-consumption of PS^* .
486 Therefore, different Cl effects may occur regarding various combinations of reactants (Figure
487 3, promoting effect in RS_A , inhibiting effects on RS_F).



488

489 Figure 4. Conceptual diagram of PS and chloride mediated ROS and RCS production, which
490 participates in the oxidation processes from S(IV) to S(VI)

491 **4 Atmospheric Implication**

492 This study provided laboratory evidence that the photosensitizers in biomass burning extracts
493 can enhance the sulfate formation in NaCl particles, primarily by triggering the formation of
494 secondary oxidants under light and air, with less contribution of direct photosensitization via
495 triplets (evidenced by N₂ atmosphere, Figure S3). The sulfate formation rate of BB_F-NaCl
496 particles were ~10 folds higher that of IS_F-NaCl, following the trends of CS_F-NaCl>RS_F-
497 NaCl>WS_F-NaCl>IS_F-NaCl. Upon UV exposure, the sulfate formation trends shifted to RS_A-
498 NaCl>CS_A-NaCl>WS_A-NaCl>IS_A-NaCl, which might be explained by the effects of chloride
499 (evidenced by aqueous reactions, Figure 3 and Table 1). Interestingly, the incorporation of Cl⁻
500 into bulk solutions increased the sulfate formation rate in RS_A, while decreased it in RS_F. This
501 seems to be different from our group's previous work where no significant sulfate formation
502 rate was found with the addition of Cl⁻ (Zhang and Chan, 2024). The difference can be
503 explained by the following reasons: 1) differences in PS/Cl⁻, the prior study might use an
504 insufficient PS/Cl⁻ ratio (2:1-1:4) while the current one significantly expands it to 1:200. 2)
505 differences in photosensitizing capacity: the former study used a strong PS, while the current
506 study focused on the real BB (using TOC as metric, with only a small portion of TOC
507 considered as PS). 3) the complexity of the reaction system, the former study focused on mixing
508 two individual species, while in real BB extracts, more complicated reactions may occur.
509 Furthermore, our results using model PS show that although additional model CHN species
510 would increase the sulfate formation by expedited H transfer via acting as H-bond acceptor, the
511 addition of chloride could inhibit the sulfate formation rate, suggesting that the RCS pathway
512 was less efficient in sulfate formation compared to ROS pathway in PS-CHN bulk system
513 (Figure S10 and S11).



514 Previous studies have detected a significant proportion of NOCs, including nitroaromatics
515 (CHON) and reduced nitrogen species (CHN) in biomass burning plumes, wildfires and
516 ambient samples (Zhong et al., 2024; Wang et al., 2017b; Song et al., 2022; Cai et al., 2020).
517 These NOCs are considered as ubiquitous contributor to BrC, and can affect global climate and
518 human health. Moreover, recent research has discovered aerosol pollution in marine
519 background regions, with high levels of NOCs when air masses are transported from wildfires
520 or biomass burning events in nearby (Zhong et al., 2024; Qin et al., 2024). These NOCs,
521 combined with reactive gases, may mix with sea-salt aerosols and impact regional air quality
522 in coastal zones. While our prior study has examined the potential interplay between chloride
523 and PS at limited mixing ratios (up to 4:1 in bulk solution) (Zhang and Chan, 2024), this work
524 expanded the Cl⁻/PS ratio to a broader range (200:1) and systematically identified the
525 interactions among different organics, including PS, NOCs, and chloride, using sulfate
526 formation as a compass. This highlights the importance to study secondary aerosol formation
527 in mixed experimental system under air pollution complex. Our work suggests that in coastal
528 regions heavily influenced by anthropogenic emissions like biomass burning, especially those
529 near the rice-growing regions or affected by transported wildfire smoke, such as Guangdong,
530 Fujian and Taiwan, the transported BB plumes together with the high RH (Cheung et al., 2015)
531 and abundant reactive gases, would play an inevitable role in sulfate and potentially secondary
532 organic aerosol formation.

533 **Data availability**

534 Datasets are available upon request to the corresponding author, Chak K. Chan
535 (chak.chan@kaust.edu.sa).

536 **Author contributions**

537 RT and CC conceptualized and designed the study. YQ and YC collected the samples. RT
538 performed the experiments, data analysis and wrote the draft. JM provided assistance in data
539 processing. All the authors reviewed, edited and contributed to the scientific discussions.

540 **Competing interests**

541 The authors declare no conflicts of interest.

542 **Acknowledgments**

543 We gratefully acknowledge the support from the Hong Kong Research Grants Council (No.
544 11314222), the National Natural Science Foundation of China (42107115), and the Natural
545 Science Foundation of Shandong Province, China (ZR2021QD111). The authors also thank the
546 University Research Facility in Chemical and Environmental Analysis (UCEA) at The Hong
547 Kong Polytechnic University for the use of its UHPLC-HESI-Orbitrap Mass Spectrometer and
548 Dr Sirius Tse and Dr Chi Hang Chow for assistance with sample analyses.

549 **References**

550 Alexander, B., Allman, D. J., Amos, H. M., Fairlie, T. D., Dachs, J., Hegg, D. A., and Sletten, R. S.:
551 Isotopic constraints on the formation pathways of sulfate aerosol in the marine boundary layer of the



- 552 subtropical northeast Atlantic Ocean, *Journal of Geophysical Research: Atmospheres*, 117,
553 <https://doi.org/10.1029/2011JD016773>, 2012.
- 554 Anastasio, C. and Newberg, J. T.: Sources and sinks of hydroxyl radical in sea-salt particles, *Journal of*
555 *Geophysical Research: Atmospheres*, 112, 2007.
- 556 Andreae, M. O.: Emission of trace gases and aerosols from biomass burning – an updated assessment,
557 *Atmos. Chem. Phys.*, 19, 8523-8546, 10.5194/acp-19-8523-2019, 2019.
- 558 Bond, T. C., Doherty, S. J., Fahey, D. W., Forster, P. M., Berntsen, T., DeAngelo, B. J., Flanner, M. G.,
559 Ghan, S., Kärcher, B., Koch, D., Kinne, S., Kondo, Y., Quinn, P. K., Sarofim, M. C., Schultz, M. G.,
560 Schulz, M., Venkataraman, C., Zhang, H., Zhang, S., Bellouin, N., Guttikunda, S. K., Hopke, P. K.,
561 Jacobson, M. Z., Kaiser, J. W., Klimont, Z., Lohmann, U., Schwarz, J. P., Shindell, D., Storelvmo, T.,
562 Warren, S. G., and Zender, C. S.: Bounding the role of black carbon in the climate system: A scientific
563 assessment, *Journal of Geophysical Research: Atmospheres*, 118, 5380-5552,
564 <https://doi.org/10.1002/jgrd.50171>, 2013.
- 565 Cai, J., Zeng, X., Zhi, G., Gligorovski, S., Sheng, G., Yu, Z., Wang, X., and Peng, P.: Molecular
566 composition and photochemical evolution of water-soluble organic carbon (WSOC) extracted from field
567 biomass burning aerosols using high-resolution mass spectrometry, *Atmos. Chem. Phys.*, 20, 6115-6128,
568 10.5194/acp-20-6115-2020, 2020.
- 569 Cao, Y., Liu, J., Ma, Q., Zhang, C., Zhang, P., Chen, T., Wang, Y., Chu, B., Zhang, X., Francisco, J. S.,
570 and He, H.: Photoactivation of Chlorine and Its Catalytic Role in the Formation of Sulfate Aerosols,
571 *Journal of the American Chemical Society*, 146, 1467-1475, 10.1021/jacs.3c10840, 2024.
- 572 Charlson, R. J., Schwartz, S. E., Hales, J. M., Cess, R. D., Coakley, J. A., Hansen, J. E., and Hofmann,
573 D. J.: Climate Forcing by Anthropogenic Aerosols, *Science*, 255, 423-430,
574 doi:10.1126/science.255.5043.423, 1992.
- 575 Chen, J., Li, C., Ristovski, Z., Milic, A., Gu, Y., Islam, M. S., Wang, S., Hao, J., Zhang, H., He, C., Guo,
576 H., Fu, H., Miljevic, B., Morawska, L., Thai, P., Lam, Y. F., Pereira, G., Ding, A., Huang, X., and Dumka,
577 U. C.: A review of biomass burning: Emissions and impacts on air quality, health and climate in China,
578 *Science of The Total Environment*, 579, 1000-1034, <https://doi.org/10.1016/j.scitotenv.2016.11.025>,
579 2017.
- 580 Chen, Y., Zheng, P., Wang, Z., Pu, W., Tan, Y., Yu, C., Xia, M., Wang, W., Guo, J., Huang, D., Yan, C.,
581 Nie, W., Ling, Z., Chen, Q., Lee, S., and Wang, T.: Secondary Formation and Impacts of Gaseous Nitro-
582 Phenolic Compounds in the Continental Outflow Observed at a Background Site in South China,
583 *Environmental Science & Technology*, 56, 6933-6943, 10.1021/acs.est.1c04596, 2022.
- 584 Cheng, S.-B., Zhou, C.-H., Yin, H.-M., Sun, J.-L., and Han, K.-L.: OH produced from o-nitrophenol
585 photolysis: A combined experimental and theoretical investigation, *The Journal of chemical physics*, 130,
586 2009.
- 587 Cheung, H. H., Yeung, M. C., Li, Y. J., Lee, B. P., and Chan, C. K.: Relative humidity-dependent HTDMA
588 measurements of ambient aerosols at the HKUST supersite in Hong Kong, China, *Aerosol Science and*
589 *Technology*, 49, 643-654, 2015.
- 590 Chi, J. W., Li, W. J., Zhang, D. Z., Zhang, J. C., Lin, Y. T., Shen, X. J., Sun, J. Y., Chen, J. M., Zhang, X.
591 Y., Zhang, Y. M., and Wang, W. X.: Sea salt aerosols as a reactive surface for inorganic and organic acidic
592 gases in the Arctic troposphere, *Atmos. Chem. Phys.*, 15, 11341-11353, 10.5194/acp-15-11341-2015,
593 2015.
- 594 Corral Arroyo, P., Aellig, R., Alpert, P. A., Volkamer, R., and Ammann, M.: Halogen activation and
595 radical cycling initiated by imidazole-2-carboxaldehyde photochemistry, *Atmospheric Chemistry and*



- 596 Physics, 19, 10817-10828, 2019.
- 597 Donaldson, D. J., Kroll, J. A., and Vaida, V.: Gas-phase hydrolysis of triplet SO₂: A possible direct route
598 to atmospheric acid formation, *Scientific Reports*, 6, 30000, 10.1038/srep30000, 2016.
- 599 Dou, J., Lin, P., Kuang, B.-Y., and Yu, J. Z.: Reactive Oxygen Species Production Mediated by Humic-
600 like Substances in Atmospheric Aerosols: Enhancement Effects by Pyridine, Imidazole, and Their
601 Derivatives, *Environmental Science & Technology*, 49, 6457-6465, 10.1021/es5059378, 2015.
- 602 Fang, Z., Deng, W., Zhang, Y., Ding, X., Tang, M., Liu, T., Hu, Q., Zhu, M., Wang, Z., Yang, W., Huang,
603 Z., Song, W., Bi, X., Chen, J., Sun, Y., George, C., and Wang, X.: Open burning of rice, corn and wheat
604 straws: primary emissions, photochemical aging, and secondary organic aerosol formation, *Atmos. Chem.*
605 *Phys.*, 17, 14821-14839, 10.5194/acp-17-14821-2017, 2017.
- 606 Felber, T., Schaefer, T., and Herrmann, H.: Five-Membered Heterocycles as Potential Photosensitizers in
607 the Tropospheric Aqueous Phase: Photophysical Properties of Imidazole-2-carboxaldehyde, 2-
608 Furaldehyde, and 2-Acetylfruran, *The Journal of Physical Chemistry A*, 124, 10029-10039,
609 10.1021/acs.jpca.0c07028, 2020.
- 610 Felber, T., Schaefer, T., He, L., and Herrmann, H.: Aromatic Carbonyl and Nitro Compounds as
611 Photosensitizers and Their Photophysical Properties in the Tropospheric Aqueous Phase, *The Journal of*
612 *Physical Chemistry A*, 125, 5078-5095, 10.1021/acs.jpca.1c03503, 2021.
- 613 Fu, H., Ciuraru, R., Dupart, Y., Passananti, M., Tinel, L., Rossignol, S., Perrier, S., Donaldson, D. J.,
614 Chen, J., and George, C.: Photosensitized Production of Atmospherically Reactive Organic Compounds
615 at the Air/Aqueous Interface, *Journal of the American Chemical Society*, 137, 8348-8351,
616 10.1021/jacs.5b04051, 2015.
- 617 Fushimi, A., Saitoh, K., Hayashi, K., Ono, K., Fujitani, Y., Villalobos, A. M., Shelton, B. R., Takami, A.,
618 Tanabe, K., and Schauer, J. J.: Chemical characterization and oxidative potential of particles emitted
619 from open burning of cereal straws and rice husk under flaming and smoldering conditions, *Atmospheric*
620 *Environment*, 163, 118-127, <https://doi.org/10.1016/j.atmosenv.2017.05.037>, 2017.
- 621 Fuzzi, S., Baltensperger, U., Carslaw, K., Decesari, S., Denier van der Gon, H., Facchini, M. C., Fowler,
622 D., Koren, I., Langford, B., Lohmann, U., Nemitz, E., Pandis, S., Riipinen, I., Rudich, Y., Schaap, M.,
623 Slowik, J. G., Spracklen, D. V., Vignati, E., Wild, M., Williams, M., and Gilardoni, S.: Particulate matter,
624 air quality and climate: lessons learned and future needs, *Atmos. Chem. Phys.*, 15, 8217-8299,
625 10.5194/acp-15-8217-2015, 2015.
- 626 Gantt, B. and Meskhidze, N.: The physical and chemical characteristics of marine primary organic
627 aerosol: a review, *Atmos. Chem. Phys.*, 13, 3979-3996, 10.5194/acp-13-3979-2013, 2013.
- 628 Gemayel, R., Emmelin, C., Perrier, S., Tomaz, S., Baboosian, V., Fishman, D., Nizkorodov, S., Dumas,
629 S., and George, C.: Quenching of ketone triplet excited states by atmospheric halides, *Environmental*
630 *Science: Atmospheres*, 1, 31-44, 2021.
- 631 Gen, M., Zhang, R., Huang, D. D., Li, Y., and Chan, C. K.: Heterogeneous SO₂ Oxidation in Sulfate
632 Formation by Photolysis of Particulate Nitrate, *Environmental Science & Technology Letters*, 6, 86-91,
633 10.1021/acs.estlett.8b00681, 2019a.
- 634 Gen, M., Zhang, R., Huang, D. D., Li, Y., and Chan, C. K.: Heterogeneous Oxidation of SO₂ in Sulfate
635 Production during Nitrate Photolysis at 300 nm: Effect of pH, Relative Humidity, Irradiation Intensity,
636 and the Presence of Organic Compounds, *Environmental Science & Technology*, 53, 8757-8766,
637 10.1021/acs.est.9b01623, 2019b.
- 638 Gómez Alvarez, E., Wortham, H., Strekowski, R., Zetzsch, C., and Gligorovski, S.: Atmospheric
639 Photosensitized Heterogeneous and Multiphase Reactions: From Outdoors to Indoors, *Environmental*



- 640 Science & Technology, 46, 1955-1963, 10.1021/es2019675, 2012.
- 641 Gong, C., Yuan, X., Xing, D., Zhang, D., Martins-Costa, M. T. C., Anglada, J. M., Ruiz-López, M. F.,
642 Francisco, J. S., and Zhang, X.: Fast Sulfate Formation Initiated by the Spin-Forbidden Excitation of
643 SO₂ at the Air–Water Interface, *Journal of the American Chemical Society*, 144, 22302-22308,
644 10.1021/jacs.2c10830, 2022.
- 645 Guo, S. and Li, H.: Photolysis of nitrophenols in gas phase and aqueous environment: a potential daytime
646 source for atmospheric nitrous acid (HONO), *Environmental Science: Atmospheres*, 3, 143-155, 2023.
- 647 Hu, W., Zhou, H., Chen, W., Ye, Y., Pan, T., Wang, Y., Song, W., Zhang, H., Deng, W., Zhu, M., Wang,
648 C., Wu, C., Ye, C., Wang, Z., Yuan, B., Huang, S., Shao, M., Peng, Z., Day, D. A., Campuzano-Jost, P.,
649 Lambe, A. T., Worsnop, D. R., Jimenez, J. L., and Wang, X.: Oxidation Flow Reactor Results in a Chinese
650 Megacity Emphasize the Important Contribution of S/IVOCs to Ambient SOA Formation,
651 *Environmental Science & Technology*, 56, 6880-6893, 10.1021/acs.est.1c03155, 2022.
- 652 Huang, G., Wang, S., Chang, X., Cai, S., Zhu, L., Li, Q., and Jiang, J.: Emission factors and chemical
653 profile of I/SVOCs emitted from household biomass stove in China, *Science of The Total Environment*,
654 842, 156940, <https://doi.org/10.1016/j.scitotenv.2022.156940>, 2022a.
- 655 Huang, R.-J., Yang, L., Shen, J., Yuan, W., Gong, Y., Ni, H., Duan, J., Yan, J., Huang, H., You, Q., and
656 Li, Y. J.: Chromophoric Fingerprinting of Brown Carbon from Residential Biomass Burning,
657 *Environmental Science & Technology Letters*, 9, 102-111, 10.1021/acs.estlett.1c00837, 2022b.
- 658 Huang, S., Wu, Z., Poulain, L., van Pinxteren, M., Merkel, M., Assmann, D., Herrmann, H., and
659 Wiedensohler, A.: Source apportionment of the organic aerosol over the Atlantic Ocean from
660 53° N to 53° S: significant contributions from marine emissions and long-range transport,
661 *Atmos. Chem. Phys.*, 18, 18043-18062, 10.5194/acp-18-18043-2018, 2018.
- 662 Hung, H.-M. and Hoffmann, M. R.: Oxidation of Gas-Phase SO₂ on the Surfaces of Acidic Microdroplets:
663 Implications for Sulfate and Sulfate Radical Anion Formation in the Atmospheric Liquid Phase,
664 *Environmental Science & Technology*, 49, 13768-13776, 10.1021/acs.est.5b01658, 2015.
- 665 Jammoul, A., Dumas, S., D'Anna, B., and George, C.: Photoinduced oxidation of sea salt halides by
666 aromatic ketones: a source of halogenated radicals, *Atmos. Chem. Phys.*, 9, 4229-4237, 10.5194/acp-9-
667 4229-2009, 2009.
- 668 Jiang, H., Carena, L., He, Y., Wang, Y., Zhou, W., Yang, L., Luan, T., Li, X., Brigante, M., Vione, D., and
669 Gligorovski, S.: Photosensitized Degradation of DMSO Initiated by PAHs at the Air–Water Interface, as
670 an Alternative Source of Organic Sulfur Compounds to the Atmosphere, *Journal of Geophysical Research:
671 Atmospheres*, 126, e2021JD035346, <https://doi.org/10.1029/2021JD035346>, 2021.
- 672 Jones, M. W., Abatzoglou, J. T., Veraverbeke, S., Andela, N., Lasslop, G., Forkel, M., Smith, A. J. P.,
673 Burton, C., Betts, R. A., van der Werf, G. R., Sitch, S., Canadell, J. G., Santín, C., Kolden, C., Doerr, S.
674 H., and Le Quéré, C.: Global and Regional Trends and Drivers of Fire Under Climate Change, *Reviews
675 of Geophysics*, 60, e2020RG000726, <https://doi.org/10.1029/2020RG000726>, 2022.
- 676 Jungwirth, P. and Tobias, D. J.: Chloride Anion on Aqueous Clusters, at the Air–Water Interface, and in
677 Liquid Water: Solvent Effects on Cl- Polarizability, *The Journal of Physical Chemistry A*, 106, 379-383,
678 10.1021/jp012059d, 2002.
- 679 Jungwirth, P. and Tobias, D. J.: Specific Ion Effects at the Air/Water Interface, *Chemical Reviews*, 106,
680 1259-1281, 10.1021/cr0403741, 2006.
- 681 Kalogridis, A. C., Popovicheva, O. B., Engling, G., Diapouli, E., Kawamura, K., Tachibana, E., Ono, K.,
682 Kozlov, V. S., and Eleftheriadis, K.: Smoke aerosol chemistry and aging of Siberian biomass burning
683 emissions in a large aerosol chamber, *Atmospheric Environment*, 185, 15-28,



- 684 <https://doi.org/10.1016/j.atmosenv.2018.04.033>, 2018.
- 685 Kim, Y. H., Warren, S. H., Krantz, Q. T., King, C., Jaskot, R., Preston, W. T., George, B. J., Hays, M. D.,
686 Landis, M. S., and Higuchi, M.: Mutagenicity and lung toxicity of smoldering vs. flaming emissions
687 from various biomass fuels: implications for health effects from wildland fires, *Environmental health*
688 *perspectives*, 126, 017011, 2018.
- 689 Kim, Y. H., Warren, S. H., Kooter, I., Williams, W. C., George, I. J., Vance, S. A., Hays, M. D., Higuchi,
690 M. A., Gavett, S. H., DeMarini, D. M., Jaspers, I., and Gilmour, M. I.: Chemistry, lung toxicity and
691 mutagenicity of burn pit smoke-related particulate matter, *Particle and Fibre Toxicology*, 18, 45,
692 10.1186/s12989-021-00435-w, 2021.
- 693 Kipp, B. H., Faraj, C., Li, G., and Njus, D.: Imidazole facilitates electron transfer from organic reductants,
694 *Bioelectrochemistry*, 64, 7-13, <https://doi.org/10.1016/j.bioelechem.2003.12.010>, 2004.
- 695 Koch, B. P. and Dittmar, T.: From mass to structure: An aromaticity index for high-resolution mass data
696 of natural organic matter, *Rapid communications in mass spectrometry*, 20, 926-932, 2006.
- 697 Laskin, A., Laskin, J., and Nizkorodov, S. A.: Chemistry of Atmospheric Brown Carbon, *Chemical*
698 *Reviews*, 115, 4335-4382, 10.1021/cr5006167, 2015.
- 699 Laskin, A., Smith, J. S., and Laskin, J.: Molecular Characterization of Nitrogen-Containing Organic
700 Compounds in Biomass Burning Aerosols Using High-Resolution Mass Spectrometry, *Environmental*
701 *Science & Technology*, 43, 3764-3771, 10.1021/es803456n, 2009.
- 702 Liang, Z., Zhou, L., Infante Cuevas, R. A., Li, X., Cheng, C., Li, M., Tang, R., Zhang, R., Lee, P. K. H.,
703 Lai, A. C. K., and Chan, C. K.: Sulfate Formation in Incense Burning Particles: A Single-Particle Mass
704 Spectrometric Study, *Environmental Science & Technology Letters*, 9, 718-725,
705 10.1021/acs.estlett.2c00492, 2022.
- 706 Lin, P., Rincon, A. G., Kalberer, M., and Yu, J. Z.: Elemental Composition of HULIS in the Pearl River
707 Delta Region, China: Results Inferred from Positive and Negative Electrospray High Resolution Mass
708 Spectrometric Data, *Environmental Science & Technology*, 46, 7454-7462, 10.1021/es300285d, 2012.
- 709 Lin, P., Fleming, L. T., Nizkorodov, S. A., Laskin, J., and Laskin, A.: Comprehensive Molecular
710 Characterization of Atmospheric Brown Carbon by High Resolution Mass Spectrometry with
711 Electrospray and Atmospheric Pressure Photoionization, *Analytical Chemistry*, 90, 12493-12502,
712 10.1021/acs.analchem.8b02177, 2018.
- 713 Lin, P., Aiona, P. K., Li, Y., Shiraiwa, M., Laskin, J., Nizkorodov, S. A., and Laskin, A.: Molecular
714 Characterization of Brown Carbon in Biomass Burning Aerosol Particles, *Environmental Science &*
715 *Technology*, 50, 11815-11824, 10.1021/acs.est.6b03024, 2016.
- 716 Liu, T. and Abbatt, J. P. D.: Oxidation of sulfur dioxide by nitrogen dioxide accelerated at the interface
717 of deliquesced aerosol particles, *Nature Chemistry*, 13, 1173-1177, 10.1038/s41557-021-00777-0, 2021.
- 718 Liu, T., Clegg, S. L., and Abbatt, J. P.: Fast oxidation of sulfur dioxide by hydrogen peroxide in
719 deliquesced aerosol particles, *Proceedings of the National Academy of Sciences*, 117, 1354-1359, 2020.
- 720 Mabato, B. R. G., Li, Y. J., Huang, D. D., Wang, Y., and Chan, C. K.: Comparison of aqueous secondary
721 organic aerosol (aqSOA) product distributions from guaiacol oxidation by non-phenolic and phenolic
722 methoxybenzaldehydes as photosensitizers in the absence and presence of ammonium nitrate, *Atmos.*
723 *Chem. Phys.*, 23, 2859-2875, 10.5194/acp-23-2859-2023, 2023.
- 724 Mabato, B. R. G., Lyu, Y., Ji, Y., Li, Y. J., Huang, D. D., Li, X., Nah, T., Lam, C. H., and Chan, C. K.:
725 Aqueous secondary organic aerosol formation from the direct photosensitized oxidation of vanillin in the
726 absence and presence of ammonium nitrate, *Atmos. Chem. Phys.*, 22, 273-293, 10.5194/acp-22-273-
727 2022, 2022.



- 728 Mao, J., Ren, X., Brune, W. H., Olson, J. R., Crawford, J. H., Fried, A., Huey, L. G., Cohen, R. C., Heikes,
729 B., Singh, H. B., Blake, D. R., Sachse, G. W., Diskin, G. S., Hall, S. R., and Shetter, R. E.: Airborne
730 measurement of OH reactivity during INTEX-B, *Atmos. Chem. Phys.*, 9, 163-173, 10.5194/acp-9-163-
731 2009, 2009.
- 732 Mauldin Iii, R. L., Berndt, T., Sipilä, M., Paasonen, P., Petäjä, T., Kim, S., Kurtén, T., Stratmann, F.,
733 Kerminen, V. M., and Kulmala, M.: A new atmospherically relevant oxidant of sulphur dioxide, *Nature*,
734 488, 193-196, 10.1038/nature11278, 2012.
- 735 Mohr, C., Lopez-Hilfiker, F. D., Zotter, P., Prévôt, A. S. H., Xu, L., Ng, N. L., Herndon, S. C., Williams,
736 L. R., Franklin, J. P., Zahniser, M. S., Worsnop, D. R., Knighton, W. B., Aiken, A. C., Gorkowski, K. J.,
737 Dubey, M. K., Allan, J. D., and Thornton, J. A.: Contribution of Nitrated Phenols to Wood Burning Brown
738 Carbon Light Absorption in Detling, United Kingdom during Winter Time, *Environmental Science &*
739 *Technology*, 47, 6316-6324, 10.1021/es400683v, 2013.
- 740 Nel, A.: Air Pollution-Related Illness: Effects of Particles, *Science*, 308, 804-806,
741 doi:10.1126/science.1108752, 2005.
- 742 Parker, K. M. and Mitch, W. A.: Halogen radicals contribute to photooxidation in coastal and estuarine
743 waters, *Proceedings of the National Academy of Sciences*, 113, 5868-5873, 2016.
- 744 Peng, Z. and Jimenez, J. L.: Radical chemistry in oxidation flow reactors for atmospheric chemistry
745 research, *Chemical Society Reviews*, 49, 2570-2616, 2020.
- 746 Pozzoli, L., Gilardoni, S., Perrone, M. G., de Gennaro, G., de Rienzo, M., and Vione, D.: POLYCYCLIC
747 AROMATIC HYDROCARBONS IN THE ATMOSPHERE: MONITORING, SOURCES, SINKS AND
748 FATE. I: MONITORING AND SOURCES, *Annali di Chimica*, 94, 17-33,
749 <https://doi.org/10.1002/adic.200490002>, 2004.
- 750 Qin, Y., Wang, H., Wang, Y., Lu, X., Tang, H., Zhang, J., Li, L., and Fan, S.: Wildfires in Southeast Asia
751 pollute the atmosphere in the northern South China Sea, *Science Bulletin*, 69, 1011-1015,
752 <https://doi.org/10.1016/j.scib.2024.02.026>, 2024.
- 753 Qiu, Y., Wu, X., Zhang, Y., Xu, L., Hong, Y., Chen, J., Chen, X., and Deng, J.: Aerosol light absorption
754 in a coastal city in Southeast China: Temporal variations and implications for brown carbon, *Journal of*
755 *Environmental Sciences*, 80, 257-266, <https://doi.org/10.1016/j.jes.2019.01.002>, 2019.
- 756 Rowe, J. P., Lambe, A. T., and Brune, W. H.: Technical Note: Effect of varying the $\lambda = 185$ and
757 254 nm photon flux ratio on radical generation in oxidation flow reactors, *Atmos. Chem. Phys.*,
758 20, 13417-13424, 10.5194/acp-20-13417-2020, 2020.
- 759 Ruiz-Lopez, M. F., Francisco, J. S., Martins-Costa, M. T. C., and Anglada, J. M.: Molecular reactions at
760 aqueous interfaces, *Nature Reviews Chemistry*, 4, 459-475, 10.1038/s41570-020-0203-2, 2020.
- 761 Safarian, M. S., Ugboya, A., Khan, I., Marichev, K. O., and Grant, K. B.: New Insights into the
762 Phototoxicity of Anthracene-Based Chromophores: The Chloride Salt Effect, *Chemical Research in*
763 *Toxicology*, 36, 1002-1020, 10.1021/acs.chemrestox.2c00235, 2023.
- 764 Salvador, C. M. G., Tang, R., Priestley, M., Li, L. J., Tsiligiannis, E., Le Breton, M., Zhu, W., Zeng, L.,
765 Wang, H., and Yu, Y.: Ambient nitro-aromatic compounds—biomass burning versus secondary formation
766 in rural China, *Atmospheric Chemistry and Physics Discussions*, 2020, 1-36, 2020.
- 767 Sangwan, M. and Zhu, L.: Absorption cross sections of 2-nitrophenol in the 295–400 nm region and
768 photolysis of 2-nitrophenol at 308 and 351 nm, *The Journal of Physical Chemistry A*, 120, 9958-9967,
769 2016.
- 770 Sangwan, M. and Zhu, L.: Role of Methyl-2-nitrophenol Photolysis as a Potential Source of OH Radicals
771 in the Polluted Atmosphere: Implications from Laboratory Investigation, *The Journal of Physical*



- 772 Chemistry A, 122, 1861-1872, 10.1021/acs.jpca.7b11235, 2018.
- 773 Schill, G. P., Froyd, K. D., Bian, H., Kupc, A., Williamson, C., Brock, C. A., Ray, E., Hornbrook, R. S.,
774 Hills, A. J., Apel, E. C., Chin, M., Colarco, P. R., and Murphy, D. M.: Widespread biomass burning smoke
775 throughout the remote troposphere, *Nature Geoscience*, 13, 422-427, 10.1038/s41561-020-0586-1, 2020.
- 776 Seinfeld, J. H. and Pandis, S. N.: *Atmospheric chemistry and physics: from air pollution to climate
777 change*, John Wiley & Sons 2016.
- 778 Song, J., Li, M., Zou, C., Cao, T., Fan, X., Jiang, B., Yu, Z., Jia, W., and Peng, P. a.: Molecular
779 Characterization of Nitrogen-Containing Compounds in Humic-like Substances Emitted from Biomass
780 Burning and Coal Combustion, *Environmental Science & Technology*, 56, 119-130,
781 10.1021/acs.est.1c04451, 2022.
- 782 Song, K., Tang, R., Li, A., Wan, Z., Zhang, Y., Gong, Y., Lv, D., Lu, S., Tan, Y., Yan, S., Yan, S., Zhang,
783 J., Fan, B., Chan, C. K., and Guo, S.: Particulate organic emissions from incense-burning smoke:
784 Chemical compositions and emission characteristics, *Science of The Total Environment*, 897, 165319,
785 <https://doi.org/10.1016/j.scitotenv.2023.165319>, 2023.
- 786 Stockwell, W. R. and Calvert, J. G.: The mechanism of the HO-SO₂ reaction, *Atmospheric Environment*
787 (1967), 17, 2231-2235, [https://doi.org/10.1016/0004-6981\(83\)90220-2](https://doi.org/10.1016/0004-6981(83)90220-2), 1983.
- 788 Tang, R., Zhang, R., Ma, J., Song, K., Mabato, B. R. G., Cuevas, R. A. I., Zhou, L., Liang, Z., Vogel, A.
789 L., Guo, S., and Chan, C. K.: Sulfate Formation by Photosensitization in Mixed Incense Burning–Sodium
790 Chloride Particles: Effects of RH, Light Intensity, and Aerosol Aging, *Environmental Science &
791 Technology*, 57, 10295-10307, 10.1021/acs.est.3c02225, 2023.
- 792 Tinel, L., Rossignol, S., Bianco, A., Passananti, M., Perrier, S., Wang, X., Brigante, M., Donaldson, D.
793 J., and George, C.: Mechanistic Insights on the Photosensitized Chemistry of a Fatty Acid at the
794 Air/Water Interface, *Environmental Science & Technology*, 50, 11041-11048, 10.1021/acs.est.6b03165,
795 2016.
- 796 Ting, Y., Mitchell, E. J. S., Allan, J. D., Liu, D., Spracklen, D. V., Williams, A., Jones, J. M., Lea-Langton,
797 A. R., McFiggans, G., and Coe, H.: Mixing State of Carbonaceous Aerosols of Primary Emissions from
798 “Improved” African Cookstoves, *Environmental Science & Technology*, 52, 10134-10143,
799 10.1021/acs.est.8b00456, 2018.
- 800 Tkacik, D. S., Lambe, A. T., Jathar, S., Li, X., Presto, A. A., Zhao, Y., Blake, D., Meinardi, S., Jayne, J.
801 T., Croteau, P. L., and Robinson, A. L.: Secondary Organic Aerosol Formation from in-Use Motor Vehicle
802 Emissions Using a Potential Aerosol Mass Reactor, *Environmental Science & Technology*, 48, 11235-
803 11242, 10.1021/es502239v, 2014.
- 804 van Pinxteren, M., Fiedler, B., van Pinxteren, D., Iinuma, Y., Körtzinger, A., and Herrmann, H.: Chemical
805 characterization of sub-micrometer aerosol particles in the tropical Atlantic Ocean: marine and biomass
806 burning influences, *Journal of Atmospheric Chemistry*, 72, 105-125, 10.1007/s10874-015-9307-3, 2015.
- 807 Wang, J., Li, J., Ye, J., Zhao, J., Wu, Y., Hu, J., Liu, D., Nie, D., Shen, F., and Huang, X.: Fast sulfate
808 formation from oxidation of SO₂ by NO₂ and HONO observed in Beijing haze, *Nature Communications*,
809 11, 2844, 2020a.
- 810 Wang, N., Zhou, D., Liu, H., Tu, Y., Ma, Y., and Li, Y.: Triplet-Excited Dissolved Organic Matter
811 Efficiently Promoted Atmospheric Sulfate Production: Kinetics and Mechanisms, *Separations*, 10, 335,
812 2023a.
- 813 Wang, T., Deng, L., Tan, C., Hu, J., and Singh, R. P.: Comparative analysis of chlorinated disinfection
814 byproducts formation from 4-nitrophenol and 2-amino-4-nitrophenol during UV/post-chlorination,
815 *Science of The Total Environment*, 927, 172200, <https://doi.org/10.1016/j.scitotenv.2024.172200>, 2024a.



- 816 Wang, W., Liu, Y., Wang, T., Ge, Q., Li, K., Liu, J., You, W., Wang, L., Xie, L., Fu, H., Chen, J., and
817 Zhang, L.: Significantly Accelerated Photosensitized Formation of Atmospheric Sulfate at the Air–Water
818 Interface of Microdroplets, *Journal of the American Chemical Society*, 146, 6580-6590,
819 10.1021/jacs.3c11892, 2024b.
- 820 Wang, W., Liu, M., Wang, T., Song, Y., Zhou, L., Cao, J., Hu, J., Tang, G., Chen, Z., Li, Z., Xu, Z., Peng,
821 C., Lian, C., Chen, Y., Pan, Y., Zhang, Y., Sun, Y., Li, W., Zhu, T., Tian, H., and Ge, M.: Sulfate formation
822 is dominated by manganese-catalyzed oxidation of SO₂ on aerosol surfaces during haze events, *Nature*
823 *Communications*, 12, 1993, 10.1038/s41467-021-22091-6, 2021.
- 824 Wang, X., Gu, R., Wang, L., Xu, W., Zhang, Y., Chen, B., Li, W., Xue, L., Chen, J., and Wang, W.:
825 Emissions of fine particulate nitrated phenols from the burning of five common types of biomass,
826 *Environmental Pollution*, 230, 405-412, <https://doi.org/10.1016/j.envpol.2017.06.072>, 2017a.
- 827 Wang, X., Gemayel, R., Hayeck, N., Perrier, S., Charbonnel, N., Xu, C., Chen, H., Zhu, C., Zhang, L.,
828 Wang, L., Nizkorodov, S. A., Wang, X., Wang, Z., Wang, T., Mellouki, A., Riva, M., Chen, J., and George,
829 C.: Atmospheric Photosensitization: A New Pathway for Sulfate Formation, *Environmental Science &*
830 *Technology*, 54, 3114-3120, 10.1021/acs.est.9b06347, 2020b.
- 831 Wang, Y., Hu, M., Xu, N., Qin, Y., Wu, Z., Zeng, L., Huang, X., and He, L.: Chemical composition and
832 light absorption of carbonaceous aerosols emitted from crop residue burning: influence of combustion
833 efficiency, *Atmos. Chem. Phys.*, 20, 13721-13734, 10.5194/acp-20-13721-2020, 2020c.
- 834 Wang, Y., Qiu, T., Zhang, C., Hao, T., Mabato, B. R. G., Zhang, R., Gen, M., Chan, M. N., Huang, D. D.,
835 and Ge, X.: Co-photolysis of mixed chromophores affects atmospheric lifetimes of brown carbon,
836 *Environmental Science: Atmospheres*, 3, 1145-1158, 2023b.
- 837 Wang, Y., Zhang, Q., Jiang, J., Zhou, W., Wang, B., He, K., Duan, F., Zhang, Q., Philip, S., and Xie, Y.:
838 Enhanced sulfate formation during China's severe winter haze episode in January 2013 missing from
839 current models, *Journal of Geophysical Research: Atmospheres*, 119, 10,425-410,440,
840 <https://doi.org/10.1002/2013JD021426>, 2014.
- 841 Wang, Y., Hu, M., Lin, P., Guo, Q., Wu, Z., Li, M., Zeng, L., Song, Y., Zeng, L., Wu, Y., Guo, S., Huang,
842 X., and He, L.: Molecular Characterization of Nitrogen-Containing Organic Compounds in Humic-like
843 Substances Emitted from Straw Residue Burning, *Environmental Science & Technology*, 51, 5951-5961,
844 10.1021/acs.est.7b00248, 2017b.
- 845 Woods, E., III, Harris, O. T., Leiter, W. E., Burner, N. E., Ofosuhen, P., Krez, A., Hilton, M. A., and
846 Burke, K. A.: Lifetime of Triplet Photosensitizers in Aerosol Using Time-Resolved Photoelectric Activity,
847 *ACS Earth and Space Chemistry*, 4, 1424-1434, 10.1021/acsearthspacechem.0c00141, 2020.
- 848 Wu, C.-H., Yuan, C.-S., Yen, P.-H., Yeh, M.-J., and Soong, K.-Y.: Diurnal and seasonal variation,
849 chemical characteristics, and source identification of marine fine particles at two remote islands in South
850 China Sea: A superimposition effect of local emissions and long-range transport, *Atmospheric*
851 *Environment*, 270, 118889, <https://doi.org/10.1016/j.atmosenv.2021.118889>, 2022.
- 852 Wyant, M. C., Bretherton, C. S., Wood, R., Carmichael, G. R., Clarke, A., Fast, J., George, R., Gustafson
853 Jr, W. I., Hannay, C., Lauer, A., Lin, Y., Morcrette, J. J., Mulcahy, J., Saide, P. E., Spak, S. N., and Yang,
854 Q.: Global and regional modeling of clouds and aerosols in the marine boundary layer during VOCALS:
855 the VOCA intercomparison, *Atmos. Chem. Phys.*, 15, 153-172, 10.5194/acp-15-153-2015, 2015.
- 856 Xie, M., Chen, X., Hays, M. D., and Holder, A. L.: Composition and light absorption of N-containing
857 aromatic compounds in organic aerosols from laboratory biomass burning, *Atmos. Chem. Phys.*, 19,
858 2899-2915, 10.5194/acp-19-2899-2019, 2019.
- 859 Yan, X., Bain, R. M., and Cooks, R. G.: Organic Reactions in Microdroplets: Reaction Acceleration



860 Revealed by Mass Spectrometry, *Angewandte Chemie International Edition*, 55, 12960-12972,
861 <https://doi.org/10.1002/anie.201602270>, 2016.

862 Yang, M., Zhang, H., Chang, F., and Hu, X.: Self-sensitized photochlorination of benzo[a]pyrene in saline
863 water under simulated solar light irradiation, *Journal of Hazardous Materials*, 408, 124445,
864 <https://doi.org/10.1016/j.jhazmat.2020.124445>, 2021.

865 Ye, C., Lu, K., Song, H., Mu, Y., Chen, J., and Zhang, Y.: A critical review of sulfate aerosol formation
866 mechanisms during winter polluted periods, *Journal of Environmental Sciences*, 123, 387-399,
867 <https://doi.org/10.1016/j.jes.2022.07.011>, 2023.

868 Zhang, L., Hu, B., Liu, X., Luo, Z., Xing, R., Li, Y., Xiong, R., Li, G., Cheng, H., Lu, Q., Shen, G., and
869 Tao, S.: Variabilities in Primary N-Containing Aromatic Compound Emissions from Residential Solid
870 Fuel Combustion and Implications for Source Tracers, *Environmental Science & Technology*, 56, 13622-
871 13633, 10.1021/acs.est.2c03000, 2022.

872 Zhang, R. and Chan, C. K.: Simultaneous formation of sulfate and nitrate via co-uptake of SO₂ and NO₂
873 by aqueous NaCl droplets: combined effect of nitrate photolysis and chlorine chemistry, *Atmos. Chem.*
874 *Phys.*, 23, 6113-6126, 10.5194/acp-23-6113-2023, 2023.

875 Zhang, R. and Chan, C. K.: Enhanced Sulfate Formation through Synergistic Effects of Chlorine
876 Chemistry and Photosensitization in Atmospheric Particles, *ACS ES&T Air*, 1, 92-102,
877 10.1021/acsestair.3c00030, 2024.

878 Zhang, R., Gen, M., Huang, D., Li, Y., and Chan, C. K.: Enhanced Sulfate Production by Nitrate
879 Photolysis in the Presence of Halide Ions in Atmospheric Particles, *Environmental Science & Technology*,
880 54, 3831-3839, 10.1021/acs.est.9b06445, 2020.

881 Zhang, T., Dong, J., Zhang, C., Kong, D., Ji, Y., Zhou, Q., and Lu, J.: Photo-transformation of
882 acetaminophen sensitized by fluoroquinolones in the presence of bromide, *Chemosphere*, 327, 138525,
883 <https://doi.org/10.1016/j.chemosphere.2023.138525>, 2023.

884 Zhang, Y., Wang, K., Tong, H., Huang, R.-J., and Hoffmann, T.: The maximum carbonyl ratio (MCR) as
885 a new index for the structural classification of secondary organic aerosol components, *Rapid*
886 *Communications in Mass Spectrometry*, 35, e9113, <https://doi.org/10.1002/rcm.9113>, 2021.

887 Zhao, R., Zhang, Q., Xu, X., Wang, W., Zhao, W., Zhang, W., and Zhang, Y.: Effect of photooxidation
888 on size distribution, light absorption, and molecular compositions of smoke particles from rice straw
889 combustion, *Environmental Pollution*, 311, 119950, <https://doi.org/10.1016/j.envpol.2022.119950>, 2022.

890 Zherebker, A., Rukhovich, G. D., Sarycheva, A., Lechtenfeld, O. J., and Nikolaev, E. N.: Aromaticity
891 Index with Improved Estimation of Carboxyl Group Contribution for Biogeochemical Studies,
892 *Environmental Science & Technology*, 56, 2729-2737, 10.1021/acs.est.1c04575, 2022.

893 Zhong, S., Liu, R., Yue, S., Wang, P., Zhang, Q., Ma, C., Deng, J., Qi, Y., Zhu, J., and Liu, C.-Q.: Peatland
894 Wildfires Enhance Nitrogen-Containing Organic Compounds in Marine Aerosols over the Western
895 Pacific, *Environmental Science & Technology*, 2024.

896 Zhou, L., Liang, Z., Mabato, B. R. G., Cuevas, R. A. I., Tang, R., Li, M., Cheng, C., and Chan, C. K.:
897 Sulfate formation via aerosol-phase SO₂ oxidation by model biomass burning photosensitizers: 3,4-
898 dimethoxybenzaldehyde, vanillin and syringaldehyde using single-particle mixing-state analysis, *Atmos.*
899 *Chem. Phys.*, 23, 5251-5261, 10.5194/acp-23-5251-2023, 2023.

900